High-Efficiency Elastic Wave Rectifier in One-Dimensional Linear Magnetoelastic Phononic Crystal Slabs by an External Magnetostatic Field

Luyang Feng,[1] Jiujiu Chen,[1,*] Hongbo Huang,[1] Shaoyong Huo,[1] Zhuhua Tan,[2,†] Xu Han,[2,‡] and Guoliang Huang[3]

[1] *State Key Laboratory of Advanced Design and Manufacturing for Vehicle Body, College of Mechanical and Vehicle Engineering, Hunan University, Changsha 410082, People's Republic of China*

[2] *School of Mechanical Engineering, Hebei University of Technology, Tianjin 300401, People's Republic of China*

[3] *Department of Mechanical and Aerospace Engineering, University Missouri, Columbia, Missouri 65211, USA*

(Received 7 January 2020; revised manuscript received 13 May 2020; accepted 18 May 2020; published 17 June 2020)

Reciprocity is a fundamental property of wave propagation in linear time-invariant media. However, it is substantially harder to break reciprocity for elastic waves in a linear elastic system with the help of a magnetostatic field, since elastic waves are spinless in nature. Here, we realize nonreciprocal elastic waves in one-dimensional linear magnetoelastic phononic crystal slabs by an external magnetostatic field. The asymmetric dispersion of spin waves, which is induced by the simultaneous breaking of the time-reversal and spatial-inversion symmetries, results in an efficient elastic wave diode effect in a periodic system due to magnetoelastic interactions. Remarkably, a bidirectional nonreciprocity of elastic waves is achieved based on the folding-back effect of the periodic structure. Our proposed scheme opens up avenues for the design of nonreciprocal devices, such as on-chip tunable diodes, rectifiers, and topological insulators.

DOI: 10.1103/PhysRevApplied.13.064042

I. INTRODUCTION

Reciprocity is a generic feature in various physical systems because it is directly associated with the symmetry of physical laws under time reversal. The breaking of reciprocity is vitally important in numerous fields, such as the control of energy flux [1–5], imaging technologies [6], and topological insulators [7–12]. For instance, electrical diodes, as a typical nonreciprocal representative in electronic systems, have already contributed to substantial scientific revolutions in many aspects, including integrated circuits, lighting, and signal indication. Motivated by electrical diodes, thermal diodes exhibiting a rectifying effect on thermal energy are achieved in nonlinear lattices [13,14]. Similarly, nonreciprocity in photonic systems can be realized by many mechanisms, such as the nonlinearity of the optical medium [15,16] and the mode conversion [17,18]. Synchronously, the concept of nonreciprocity further extends to phononic systems. The main means to achieve acoustic nonreciprocity are based on the nonlinearity of an acoustic material [2,3,19–22], the local circulation of a fluid [6], and the space-time modulation of acoustic characteristics [23–27]. However, the nonlinear approach introduces an inherently low conversion efficiency and other dynamic schemes have difficulties in application at high-speed modulation or on the nanoscale, which have severe limitations for practical application of nonreciprocity.

The interaction between many subsystems, as another excellent way to induce the nonreciprocity of classical waves in linear static systems, is studied extensively from optomechanical coupling [28–30] to acousto-optic coupling [31,32]. Especially, the Faraday effect, which is the polarization rotation of light after passing through a medium in a magnetic field, is utilized to achieve optical nonreciprocity in photonic systems [33–38]. Similarly, one expects to extend the concept to phononic systems. For acoustic waves, the conventional spin-orbital interaction under a magnetic field cannot break the reciprocity due to the intrinsic longitudinal nature of sound polarization. Fortunately, the analog of the Faraday effect for elastic waves is demonstrated in magnetic materials [39–41]. However, the corresponding Faraday effect is so weak that the realization of an efficient elastic wave diode based on this phenomenon still remains an even greater challenge. It is highly desirable to develop an efficient strategy for the nonreciprocity of elastic waves in linear systems by an external magnetostatic field.

The purpose of this article is to realize nonreciprocal elastic waves in a linear static system. We develop a rigorous theoretical framework to describe the propagation of spin and elastic waves in the presence of magnetoelastic

*jjchen@hnu.edu.cn
†zhtan@hnu.edu.cn
‡hanxu@hnu.edu.cn

interactions in one-dimensional (1D) linear magnetoelastic phononic crystal (PC) slabs and calculate the corresponding band structure by the plane-wave expansion method. It is demonstrated that, due to magnetoelastic interactions, the asymmetric dispersion of spin waves in the parity-time symmetry-broken periodic system can lead to an efficient elastic wave diode effect that is absent in the nonperiodic system. Furthermore, we can tune *in situ* the frequency of the nonreciprocity of elastic waves by simply changing the value of the controllable external magnetostatic field without altering the structure, which allows nonreciprocal devices to operate within a wider frequency range.

II. MODEL AND THEORY

As shown in Fig. 1, the 1D magnetoelastic PC slabs are constructed by stacking alternating layers A (marked in cyan) and B (yellow) with the normal of their planes parallel to the x_1 axis. An external magnetostatic field, H, is applied to the whole PC slabs along the x_3 axis, resulting in the time-reversal symmetry of the spin wave subsystem being broken over the whole PC slabs because magnetization precesses only clockwise around its equilibrium direction in magnetized magnetoelastic materials. Due to magnetoelastic interactions, the time-reversal symmetry of the elastic wave subsystem is also broken throughout the whole PC slabs. The signs p_1 and p_2 denote the lower and upper surface-spin-pinning parameters, respectively, which are dimensionless [42,43] (see Appendix A). The lattice constant is $a = 2d = 670\,\text{nm}$, where d is the width of a single layer A or B. The thickness of the PC slabs is $h = a/2$. The materials of layers A and B are Permalloy and cobalt, respectively. The material parameters used in the calculation are chosen as follows: density $\rho = 8720\,\text{kg/m}^3$, saturation magnetization $M_S = 760\,\text{kA/m}$, exchange constant $A = 13\,\text{pJ/m}$, magnetoelastic constant $b_2 = -0.9\,\text{MJ/m}^3$, and elastic constant $c_{44} = 50\,\text{GPa}$ for Permalloy; $\rho = 8900\,\text{kg/m}^3$, $A = 20\,\text{pJ/m}$, $b_2 = 10\,\text{MJ/m}^3$, and $c_{44} = 80\,\text{GPa}$ for cobalt [44].

Neglecting relaxation of the spin wave subsystem, the Lagrangian density for an isotropic magnetoelastic solid with cubic symmetry under the magnetostatic approximation can be given by [45–47]

$$\begin{aligned} L = {} & \frac{1}{\omega_M} m_2 \dot{m}_1 - \frac{\mu_0 \omega_H}{2\omega_M}(m_1^2 + m_2^2) - \frac{D}{2\omega_M}(\nabla^2 m_1 + \nabla^2 m_2) \\ & + \frac{\mu_0}{2}\sum_i \frac{\partial^2 \phi}{\partial x_i^2} - \mu_0\left(m_1 \frac{\partial \phi}{\partial x_1} + m_2 \frac{\partial \phi}{\partial x_2}\right) \\ & + \frac{1}{2}\rho \sum_i \dot{u}_i^2 - \left[c_{44}\sum_{ij} e_{ij}^2 + \frac{1}{2} c_{12}\Big(\sum_i e_{ii}\Big)^2\right] \\ & + \frac{b_2}{M_S}[m_1(e_{13} + e_{31}) + m_2(e_{23} + e_{32})], \end{aligned} \tag{1}$$

where $\omega_M = \gamma M_S$, $\omega_H = \gamma H$, $D = 2\gamma A / M_S$, and $e_{ij} = (\partial u_i / \partial x_j + \partial u_j / \partial x_i)/2$. γ, μ_0, x_i, m_i, u_i, φ, and c_{ij} are the gyromagnetic ratio, the magnetic susceptibility of a vacuum, the component of Eulerian coordinates, the dynamic magnetization component, the displacement component, the magnetic potential, and the component of the elastic tensor, respectively. On the right-hand side of Eq. (1), the first two terms are the Zeeman energy density; the third term represents the exchange energy density; the fourth and fifth terms denote the electromagnetic field energy density; the sixth and seventh terms are the elastic energy density; and the last term represents the magnetoelastic coupling energy density in the linear approximation.

The Lagrangian equations of motion can be expressed as

$$\frac{\partial L}{\partial \psi_j} - \frac{d}{dt}\frac{\partial L}{\partial \dot{\psi}_j} - \sum_i \frac{\partial}{\partial x_i}\frac{\partial L}{\partial(\partial \psi_j / x_i)} = 0, \tag{2}$$

where ψ_j can represent any one of the fields (m_1, m_2, u_1, u_2, u_3, φ) in Eq. (1). When the field ψ_j is regarded as m_1, m_2, u_1, u_2, u_3, and φ in turn, the following equations can be obtained from Eqs. (1) and (2):

$$\begin{aligned} \dot{m}_1 = {} & \gamma\mu_0 H m_2 + \gamma\mu_0 M_S \frac{\partial \phi}{\partial x_2} - \omega_M \sum_i \frac{\partial}{\partial x_i}\left(\frac{D}{\omega_M}\frac{\partial m_2}{\partial x_i}\right) \\ & + \gamma b_2(e_{23} + e_{32}), \end{aligned} \tag{3}$$

$$\begin{aligned} \dot{m}_2 = {} & -\gamma\mu_0 H m_1 - \gamma\mu_0 M_S \frac{\partial \phi}{\partial x_1} + \omega_M \sum_i \frac{\partial}{\partial x_i}\left(\frac{D}{\omega_M}\frac{\partial m_1}{\partial x_i}\right) \\ & - \gamma b_2(e_{13} + e_{31}), \end{aligned} \tag{4}$$

$$\begin{aligned} \rho \ddot{u}_1^2 = {} & \sum_i \frac{\partial}{\partial x_i}\left(c_{44}\frac{\partial u_1}{\partial x_i}\right) + \frac{\partial}{\partial x_1}[(c_{44} + c_{12})\nabla \cdot \vec{u}] \\ & + \frac{\partial}{\partial x_3}\left(\frac{b_2}{M_S} m_1\right), \end{aligned} \tag{5}$$

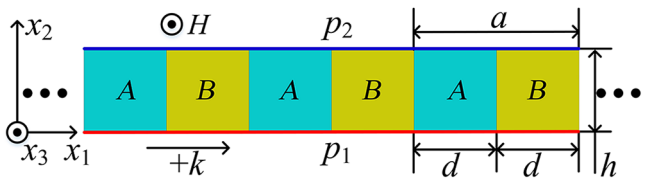

FIG. 1. Schematic of 1D magnetoelastic PC slabs. Lower and upper surface-spin-pinning parameters are marked by p_1 and p_2, respectively. External magnetostatic field H is applied along the x_3 axis.

$$\rho\ddot{u}_2^2 = \sum_i \frac{\partial}{\partial x_i}\left(c_{44}\frac{\partial u_2}{\partial x_i}\right) + \frac{\partial}{\partial x_2}[(c_{44}+c_{12})\nabla\cdot\vec{u}] + \frac{\partial}{\partial x_3}\left(\frac{b_2}{M_S}m_2\right), \tag{6}$$

$$\rho\ddot{u}_3^2 = \sum_i \frac{\partial}{\partial x_i}\left(c_{44}\frac{\partial u_3}{\partial x_i}\right) + \frac{\partial}{\partial x_3}[(c_{44}+c_{12})\nabla\cdot\vec{u}] + \frac{\partial}{\partial x_1}\left(\frac{b_2}{M_S}m_1\right) + \frac{\partial}{\partial x_2}\left(\frac{b_2}{M_S}m_2\right), \tag{7}$$

$$-\sum_i \frac{\partial^2\phi}{\partial x_i^2} + \frac{\partial m_1}{\partial x_1} + \frac{\partial m_2}{\partial x_2} = 0. \tag{8}$$

In our system, for spin and elastic waves propagating along the x_1 axis, Eqs. (3)–(8) can be simplified as

$$\dot{m}_1 = \gamma\mu_0 H m_2 + \gamma\mu_0 M_S\frac{\partial\phi}{\partial x_2} - \omega_M\frac{\partial}{\partial x_1}\left(\frac{D}{\omega_M}\frac{\partial m_2}{\partial x_1}\right) - \omega_M\frac{\partial}{\partial x_2}\left(\frac{D}{\omega_M}\frac{\partial m_2}{\partial x_2}\right) + \gamma b_2\frac{\partial u_3}{\partial x_2}, \tag{9}$$

$$\dot{m}_2 = -\gamma\mu_0 H m_1 - \gamma\mu_0 M_S\frac{\partial\phi}{\partial x_1} + \omega_M\frac{\partial}{\partial x_1}\left(\frac{D}{\omega_M}\frac{\partial m_1}{\partial x_1}\right) + \omega_M\frac{\partial}{\partial x_2}\left(\frac{D}{\omega_M}\frac{\partial m_1}{\partial x_2}\right) - \gamma b_2\frac{\partial u_3}{\partial x_1}, \tag{10}$$

$$\rho\ddot{u}_3 = \frac{\partial}{\partial x_1}\left(c_{44}\frac{\partial u_3}{\partial x_1}\right) + \frac{\partial}{\partial x_2}\left(c_{44}\frac{\partial u_3}{\partial x_2}\right) + \frac{\partial}{\partial x_1}\left(\frac{b_2}{M_S}m_1\right) + \frac{\partial}{\partial x_2}\left(\frac{b_2}{M_S}m_2\right), \tag{11}$$

$$-\frac{\partial^2\phi}{\partial x_1^2} - \frac{\partial^2\phi}{\partial x_2^2} + \frac{\partial m_1}{\partial x_1} + \frac{\partial m_2}{\partial x_2} = 0. \tag{12}$$

Here, we omit the simplified forms of Eqs. (5) and (6) due to the absence of coupling with the other equations.

The plane-wave expansion method is used for solving Eqs. (9)–(12) for the 1D magnetoelastic PC slabs [48,49]. Owing to the structure periodicity, all periodic parameters are expanded into a Fourier series. Especially, by combining Bloch's theorem, the field ψ_j can be expressed as $\psi_j = \sum_G e^{i(k+G)x-i\omega t}(A_j^G e^{ik_2x_2})$, where G is the 1D reciprocal-lattice vector, A_j^G is the amplitude vector of the field ψ_j, k is a Bloch wave vector along the x_1 direction, and k_2 is the wave number along the x_2 direction. Substituting the expanding form of the field ψ_j into Eqs. (9)–(12), we can obtain homogenous linear equations to determine both A_j^G and k_2 [50]. To ensure satisfactory convergence, we choose $n = 33$ reciprocal-lattice vectors in the computations. For spin and elastic waves in the 1D magnetoelastic PC slabs, the field used in boundary conditions can be given by $\psi_j = \sum_G e^{i(k+G)x-i\omega t}\left[\sum_{l=1}^{8n} A_j^{(l)} e^{ik_2^{(l)}x_2}\right]$.

Next, we introduce the boundary conditions of spin and elastic waves in the 1D magnetoelastic PC slabs (see Appendix B). It is well known that the surface of a slab is stress free, which can be expressed as [46]

$$T_{32}|_{x_2=0,h} = c_{44}\frac{\partial u_3}{\partial x_2} + \frac{b_2}{M_S}m_2\Big|_{x_2=0,h} = 0. \tag{13}$$

Here, we consider the influence of surface-spin pinning on spin and elastic waves. The standard forms of boundary conditions of the surface-spin pinning can be given by [42,51]

$$\pm\lambda\frac{\partial m_1}{\partial x_2} + m_1\Big|_{x_2=0,h} = 0, \tag{14}$$

$$\pm\lambda\frac{\partial m_2}{\partial x_2} + m_2\Big|_{x_2=0,h} = 0, \tag{15}$$

where $+(-)$ of the sign $\pm$ is for the surface at $x_2 = 0(h)$. Here, $\lambda = p\sqrt{c_{44}/\rho}/(\gamma\mu_0 H)$, where p is the surface-spin-pinning parameter [43].

The electromagnetic conditions that both the transverse components of magnetic field intensity and the normal components of magnetic induction intensity are continuous can be combined to obtain [43,51]

$$\sum_G[-ik_2\phi^{(l)} \pm i\sqrt{-(|k|+G')^2}\phi^{(l)} + m_2^{(l)}]\Big|_{x_2=0,h} = 0, \tag{16}$$

where $+$ and $-$ of the sign $\pm$ come from the $x_2 = 0$ and $x_2 = h$ surfaces, respectively. Note that the stress, field ψ_j, transverse components of the magnetic field intensity, and normal components of the magnetic induction intensity are continuous at the interface between magnetoelastic layers A and B, which is embedded in the structure function and periodic boundary conditions of the plane-wave expansion method [50,52]. For simplicity, the spins are assumed to be free at the interface and the influence of the interface effect [53,54] is neglected. Equations (13)–(16) can be converted into $8n$ homogeneous linear equations. When the modulus of their matrix determinant is a minimum, the corresponding values f and k are adopted to obtain the band structure of the current system.

III. RESULTS AND DISCUSSION

To realize the nonreciprocity of elastic waves, we calculate the band structure of the 1D magnetoelastic PC slabs with an applied external magnetostatic field of $H = 100$ kA/m and different surface-spin-pinning parameters of $p_1 = 0.5$ and $p_2 = 2.5$, as shown in Fig. 2(a). The red and blue lines denote spin and elastic waves, respectively. The branches of the spin and first elastic waves possess four crossing points, which are labeled as $C0$, $C0'$, $C1$, and $C1'$. $C0$ and $C0'$ are the codirectional crossing points where the spin wave and elastic wave modes have the same signs of group velocities, indicating the occurrence of mode veering, while $C1$ and $C1'$ are the contradirectional crossing points, where the two corresponding modes have opposite signs of group velocities, meaning that mode locking occurs [55]. The contradirectional crossing points are achieved by the reversal of the group velocity of spin waves induced by the folding-back effect of the periodic structure. It is noted that the current system is drastically different from the homogeneous magnetoelastic slab, where contradirectional crossing points do not exist (see Appendix C). It can be observed that the contradirectional crossing points $C1$ and $C1'$ are located at different frequency positions because of the asymmetric dispersion of spin waves for wave vectors $+k$ and $-k$ under the simultaneous breaking of the time-reversal and spatial-inversion symmetries of the spin wave system [56–58]. To more intuitively observe the contradirectional crossing points $C1$ and $C1'$, we plot an enhanced view in Fig. 2(b). Obviously, there are two directional band gaps (from 11.548 to 11.716 GHz for $+k$ and from 11.168 to 11.336 GHz for $-k$) due to the existence of magnetoelastic interactions when both the wavelengths and frequencies of the spin and elastic waves are close [44,45]. The directional band gap for either $+k$ or $-k$ indicates that the elastic waves propagating in one direction are prohibited completely, while elastic waves traveling in the opposite direction are unaffected. Therefore, an elastic wave diode effect can be obtained in the parity-time symmetry-broken periodic magnetoelastic system. It is worth emphasizing that efficient elastic wave isolation, resulting from the directional band gaps near the contradirectional anticrossing points, is significantly different from asymmetric propagation arising from the veerings in the vicinity of the codirectional anticrossing points (see Appendix C and D). In addition, the two directional band gaps for $+k$ and $-k$ have different frequency ranges, meaning that a bidirectional nonreciprocity of elastic waves exists in the current system. Notably, because the folding-back effect of the periodic structure can induce more contradirectional anticrossing points in the higher frequency range, nonreciprocal elastic waves may occur in multiple frequency regions. To further explore the impact of a reversal of spatial-inversion symmetry breaking on nonreciprocal elastic waves, we

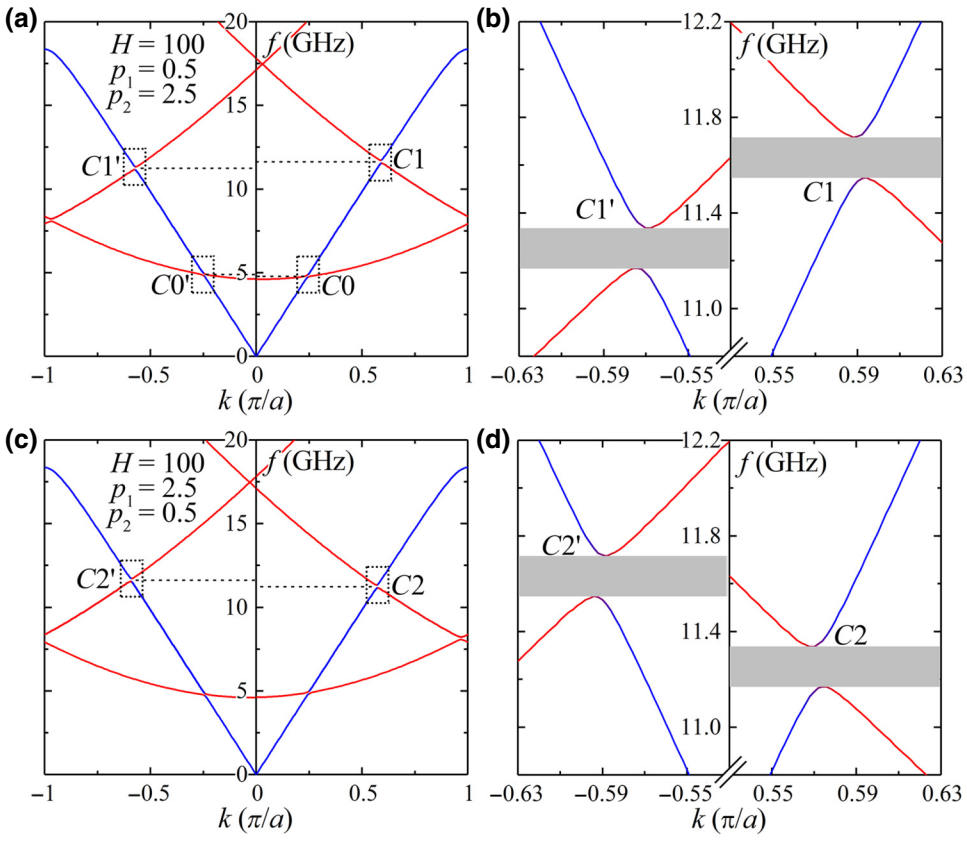

FIG. 2. (a) Band structure of 1D magnetoelastic PC slabs with $H = 100$ kA/m and different surface-spin-pinning parameters, $p_1 = 0.5$ and $p_2 = 2.5$. Red and blue lines denote spin and elastic waves, respectively. Gray areas represent directional band gaps. (b) Magnification of contradirectional anticrossing points $C1$ and $C1'$ [marked by dashed rectangles in (a)]. (c) Band structure of 1D magnetoelastic PC slabs with $H = 100$ kA/m and reversed surface-spin-pinning parameters $p_1 = 2.5$ and $p_2 = 0.5$. (d) Enlarged views of contradirectional anticrossing points $C2$ and $C2'$.

calculate the band structure of the 1D magnetoelastic PC slabs with an applied external magnetostatic field of $H = 100\,\mathrm{kA/m}$ and inverted surface-spin-pinning parameters of $p_1 = 2.5$ and $p_2 = 0.5$, as displayed in Fig. 2(c). The corresponding enlarged views of the contradirectional anticrossing points ($C2$ and $C2'$) are shown in Fig. 2(d). Compared with the band structure in Figs. 2(a) and 2(b), the dispersion of the current system flips with respect to the coordinate axis ($k = 0$), suggesting a reversal of the nonreciprocity of elastic waves. The results can be explained by the nonreciprocity being reversed under a reversal of spatial-inversion symmetry breaking due to the symmetry origin of nonreciprocity [59]. It is worth noting that the high-frequency crossings at a frequency of 17.46 GHz occur for $+k$ in Fig. 2(a), but for $-k$ in Fig. 2(c) this is due to a reversal of spatial-inversion symmetry breaking. In contrast to a dynamic nonreciprocal system based on the local circulation of fluid or space-time modulation, the current static nonreciprocal system has unique advantages of miniaturization and stability [4], and thus, has potential applications including nanoscale elastic wave diodes and on-chip topological insulators (see Appendix A).

Next, we discuss that the nonreciprocity of elastic waves cannot happen when the current system possesses spatial-inversion symmetry. The lower and upper surface-spin-pinning parameters of the current system are set to the same value ($p_1 = p_2 = 0.5$). Figures 3(a) and 3(b) display the corresponding band structure of the system under an external magnetostatic field of $H = 100\,\mathrm{kA/m}$ and an enlarged view of its contradirectional anticrossing points ($C3$ and $C3'$), respectively. It can be seen from Fig. 3(a) that contradirectional anticrossing points $C3$ and $C3'$ are located at the same frequency position because of the same absolute value of the phase velocities of the spin waves. Moreover, Fig. 3(b) shows that the directional band gaps for $+k$ and $-k$ are the same, implying that elastic wave propagation along the opposite direction is simultaneously prohibited in the same frequency range. The results confirm that elastic waves are reciprocal in the 1D magnetoelastic PC slabs with spatial-inversion symmetry.

We then explore why the nonreciprocity of elastic waves cannot also occur in the magnetoelastic periodic system possessing time-reversal symmetry. A sufficiently small external magnetostatic field ($H \to 0$) is applied to the current system, so that it is treated as an equivalent time-reversal symmetry system [56,58]. Figure 3(c) presents the corresponding band structure of the system with different surface-spin-pinning parameters, $p_1 = 0.5$ and $p_2 = 2.5$, and an enlarged view of the contradirectional anticrossing points ($C4$ and $C4'$) is plotted in Fig. 3(d). It can be observed that the directional band gaps for $+k$ and $-k$ are almost the same, which means that the elastic waves are reciprocal. Therefore, both the time-reversal and spatial-inversion symmetry breakings of the

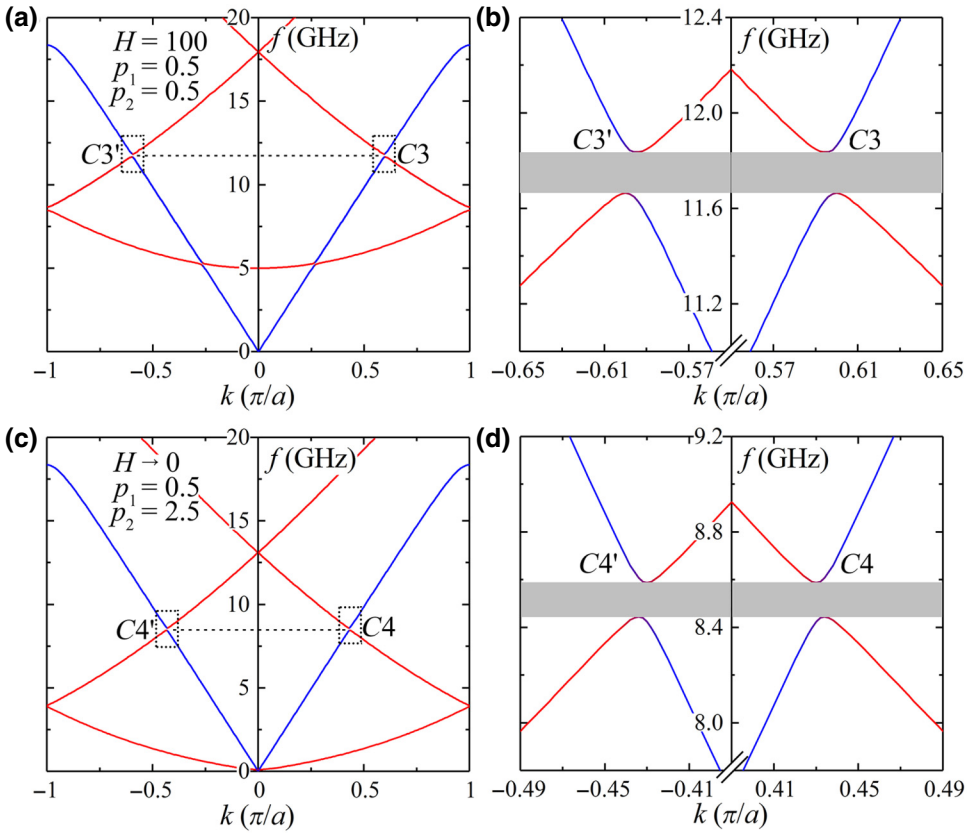

FIG. 3. (a) Band structure of 1D magnetoelastic PC slabs with $H = 100\,\mathrm{kA/m}$ and the same surface-spin-pinning parameters, $p_1 = p_2 = 0.5$. (b) Magnification of contradirectional anticrossing points $C3$ and $C3'$. (c) Band structure of 1D magnetoelastic PC slabs with sufficiently small external magnetostatic field ($H \to 0\,\mathrm{kA/m}$) and different surface-spin-pinning parameters, $p_1 = 0.5$ and $p_2 = 2.5$. (d) Enlarged views of contradirectional anticrossing points $C4$ and $C4'$.

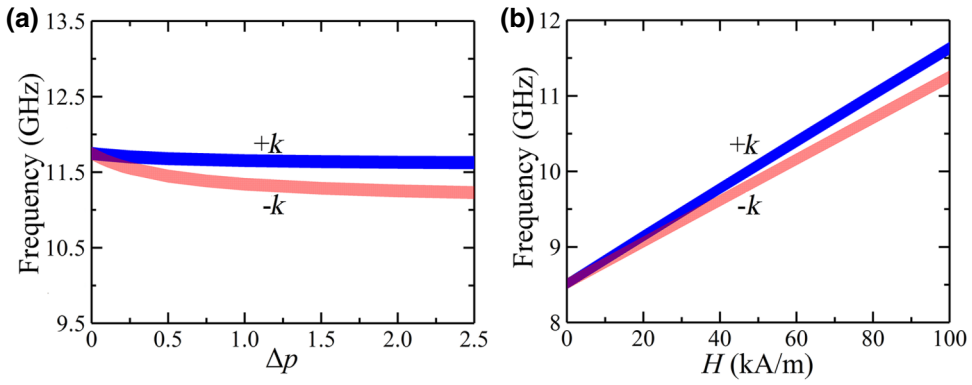

FIG. 4. Positions and widths of directional band gaps for $+k$ and $-k$ in 1D magnetoelastic PC slabs with $H = 100\,\mathrm{kA/m}$ as a function of the difference between the lower and upper surface-spin-pinning conditions ($\Delta p = p_2 - p_1$) (a), and with different surface-spin-pinning parameters ($p_1 = 0.5$ and $p_2 = 2.5$) as a function of external magnetostatic field H (b).

magnetoelastic system are necessary for nonreciprocal elastic waves in a periodic system (see Appendix E). It can be implied that, under an external magnetostatic field, bulk elastic waves in an infinite magnetoelastic structure are reciprocal because of the existence of spatial-inversion symmetry, whereas both surface elastic waves in a semi-infinite magnetic medium and elastic guided waves in a magnetoelastic plate with asymmetry about its mid-plane may be nonreciprocal, owing to breaking of the spatial-inversion symmetry [44,47,60].

To better understand the nonreciprocity of elastic waves, we investigate the impact of the difference between the lower and upper surface-spin-pinning conditions ($\Delta p = p_2 - p_1$) on directional band gaps in the 1D linear magnetoelastic PC slabs. Figure 4(a) presents the directional band gaps for $+k$ and $-k$ in the system with an external magnetic field of $H = 100\,\mathrm{kA/m}$ as a function of Δp ($p_1 = 0.5$ is unchanged). It can be observed that the widths of the directional band gaps remain almost unchanged, but their midgap frequencies decrease with an increase of Δp. In addition, the overlapping and separate processes of the two directional band gaps can be observed with increasing Δp, passing through a transition point at $\Delta p = 0.3$. It can be explained that the spatial-inversion symmetry of the current system is broken more intensely when Δp increases, which leads to a greater difference in the frequency positions of the two directional band gaps. Therefore, we can realize the nonreciprocity of elastic waves in different frequency ranges in the 1D linear magnetoelastic PC slabs by designing different surface-spin-pinning conditions.

The tunability of the systems is the cornerstone behind signal-processing systems and phononic functional devices. To observe the tunability of the nonreciprocity of elastic waves, we investigate the influence of the controllable external magnetostatic field on directional band gaps. Figure 4(b) depicts the widths and positions of the directional band gaps for $+k$ and $-k$ in the 1D magnetoelastic PC slabs with different surface-spin-pinning parameters ($p_1 = 0.5$ and $p_2 = 2.5$) as a function of the external magnetostatic field H. It can be seen that the widths of the directional band gaps remain almost unchanged, but their midgap frequencies increase gradually with increasing H. Moreover, the overlapping and separate processes of the two directional band gaps can be observed with increasing H, passing through a transition point at $H = 38.4\,\mathrm{kA/m}$. It can be explained that the time-inversion symmetry of the spin wave subsystem is broken more intensely when the external magnetostatic field increases [58], which gives rise to the greater difference in the frequency positions of the two directional band gaps. Therefore, the frequency of the nonreciprocity of elastic waves can be tuned by varying only the amplitude of the controllable external magnetostatic field, without altering the structure, which can be employed for designing tunable nonreciprocal devices, such as magnetically controlled elastic wave diodes.

Finally, an experimental prefigure of 1D magnetoelastic PC slabs is currently being considered to demonstrate the nonreciprocity of elastic waves in practice. First, the experimental sample can be fabricated by advanced nanofabrication techniques [61,62], but, so far it is challenging for the sample to obtain precise surface-spin-pinning parameters. Second, experiments are conducted on the sample to acquire its band structure [62,63]. The main experimental steps can be as follows: a vibration is excited by a needle, the sharp tip of which is pressed on the upper surface of the sample and the bottom of which is fixed on a piezoelectric ceramic disk controlled by a network analyzer. Then, the corresponding displacement field is accurately measured by scanning a laser vibrometer through the upper surface of the sample and is recorded by the network analyzer. Further, from data of the scanned displacement field, we can obtain the band structure by performing Fourier transformation. To avoid random errors, the experimental results are averaged over 20 data acquisitions.

IV. CONCLUSION

We derive a theoretical model for calculating band structures of spin and elastic waves in the presence of magnetoelastic interactions in 1D linear PC slabs that exhibit tunable nonreciprocal elastic waves. It is demonstrated that, because of magnetoelastic interactions, efficient elastic

wave isolation is achieved by the folding-back effect of the periodic structure in the parity-time symmetry-broken system, which is clearly distinguished from asymmetric propagation in a homogeneous magnetoelastic structure. Moreover, the flexibility of the system is enhanced because the operational frequencies are tunable by simply varying the value of the controllable external magnetostatic field without altering the structure. Different from previously proposed nonreciprocal systems, depending on the nonlinear effect and dynamic elements, this current model is a linear static elastic system, with advantages of high conversion efficiency, miniaturization, and stability. Furthermore, the platform can be easily extended to the field of topology for utilization in the design of an elastic analog of the quantum Hall effect. Our approach paves the way for research into nonreciprocity under an external magnetostatic field in an elastic system, which has potential applications, such as rectification, vibration and noise reduction, sensing, and bioimaging.

ACKNOWLEDGMENTS

The authors gratefully acknowledge financial support from the National Science Foundation of China under Grants No. 11374093 and No. 11672214, the Young Scholar fund sponsored by the common university and college of the province in Hunan, and the Foundation of Hubei Key Laboratory of Hydroelectric Machinery Design and Maintenance of China Three Gorges University (Grant No. 2019KJX02).

APPENDIX A: THE SURFACE-SPIN-PINNING PARAMETER

Surface-spin pinning is related to the energy status of surface spins, specifically to the degree of freedom of their precession [64–66]. The surface-spin-pinning parameter is a quantity that denotes the degree of pinning of the surface spins. In the microscopic theory of spin waves, the value of the surface-spin-pinning parameter is related to the dot product between magnetization M and the effective surface anisotropy field K_{surf} acting on the surface spins [67–71]. Based on the relation between the dot product and zero, surface pinning is divided into the main three situations: surface pinned, surface natural, and surface unpinned. In addition, the surface anisotropy field M can be affected by the charge-carrier (hole) concentration on the surface of magnetic materials and the lattice mismatch caused by an additional structure on the surface [72]. Therefore, tuning the surface anisotropy field M by doping or coating can induce different surface-spin-pinning parameters, ranging from 0.5 to 2.5 in our system. Similar to the photonic and phononic topological insulators achieved based on the z-direction inversion symmetry breaking [73–75], breaking the z-direction inversion symmetry by setting different pinning parameters on the upper or lower surfaces of the magnetoelastic medium can be used for designing an on-chip tunable magnetic topological insulator in future research.

APPENDIX B: BOUNDARY CONDITIONS OF SPIN AND ELASTIC WAVES IN 1D MAGNETOELASTIC PC SLABS

Here, we derive the boundary conditions of spin and elastic waves in 1D magnetoelastic PC slabs. The elastic boundary condition is that the surface of the PC slabs is stress free. The relevant element of the stress tensor is equal to zero at the surface, which can be expressed as [46]

$$\begin{aligned} T_{32}|_{x_2=0,h} = \frac{\partial}{\partial e_{32}} \Big\{ & \frac{1}{2}\rho \sum_i \dot{u}_i^2 + \frac{1}{2}c_{11}(e_{11}^2 + e_{22}^2 + e_{33}^2) \\ & + \frac{1}{2}c_{12}(e_{11}e_{22} + e_{22}e_{33} + e_{33}e_{11}) \\ & + 2c_{44}(e_{12}^2 + e_{23}^2 + e_{31}^2) + \frac{b_2}{M_S}[m_1(e_{13} + e_{31}) \\ & + m_2(e_{23} + e_{32})]\Big\}|_{x_2=0,h} = 0. \end{aligned} \tag{B1}$$

By simplifying this, we can obtain

$$T_{32}|_{x_2=0,h} = c_{44}\frac{\partial u_3}{\partial x_2} + \frac{b_2}{M_S}m_2\Big|_{x_2=0,h} = 0. \tag{B2}$$

Next, we describe the spin-pinning boundary condition. Its phenomenological form is defined as [42,51]

$$\pm\lambda\frac{\partial M}{\partial x_2} + M\Big|_{x_2=0,h} = 0, \tag{B3}$$

where the $+(-)$ of the sign $\pm$ is for the surface at $x_2 = 0(h)$. Replacing M with m_1 or m_2, the following forms are obtained:

$$\pm\lambda\frac{\partial m_1}{\partial x_2} + m_1\Big|_{x_2=0,h} = 0, \tag{B4}$$

$$\pm\lambda\frac{\partial m_2}{\partial x_2} + m_2\Big|_{x_2=0,h} = 0. \tag{B5}$$

The remaining electromagnetic boundary conditions are that both the transverse components of magnetic field intensity and the normal components of magnetic induction intensity are continuous, which can be written as [46]

$$\phi = \bar{\phi}, \tag{B6}$$

$$-\frac{\partial\phi}{\partial x_2} + m_2 = -\frac{\partial\bar{\phi}}{\partial x_2}, \tag{B7}$$

where $\bar{\phi}$ is the magnetic potential in a vacuum.

In the region outside the 1D magnetoelastic PC slabs, the magnetic field obeys the following Maxwell equation:

$$\nabla\bar{B} = \nabla\bar{H} = 0, \tag{B8}$$

where $\bar{B} = \mu_0\bar{H}$and $\bar{H} = -\nabla\bar{\phi}$.

In a vacuum, there is a magnetic field that is created by the spins inside the PC slabs. The field decays exponentially away from the PC slabs. The vacuum can be treated as a virtual periodic structure that has the same period and filling fraction as that of the PC slabs. As a result, the field can be given by

$$\bar{\phi} = \sum_G e^{i(k+G)x-i\omega t}\left[\sum_{l=1}^{8n} A^{(l)} e^{i\bar{k}_2^{(l)}x_2}\right]. \tag{B9}$$

Combining Eqs. (A6)–(A9), we have [43,51]

$$\sum_G [-ik_2\phi^{(l)} \pm i\sqrt{-(|k|+G')^2}\phi^{(l)} + m_2^{(l)}]\Big|_{x_2=0,h} = 0, \tag{B10}$$

where + and − of the sign ± come from the $x_2 = 0$ and $x_2 = h$ surfaces, respectively.

APPENDIX C: ASYMMETRIC PROPAGATION OF ELASTIC WAVES IN A HOMOGENEOUS MAGNETOELASTIC SLAB BY AN EXTERNAL MAGNETOSTATIC FIELD

Here, we investigate a homogeneous magnetoelastic slab with thickness $h = a/2 = 335$ nm, which is filled with Permalloy. Figure 5(a) shows the band structure of the system, with external magnetostatic field $H = 100$ kA/m and different surface-spin-pinning parameters, $p_1 = 0.5$ and $p_2 = 2.5$. It can be seen that the spin and elastic wave branches cross at different frequencies because of the asymmetric dispersion of spin waves in the parity-time symmetry-broken system [56–58]. It is noted that contradirectional crossing points do not exist in the homogeneous magnetoelastic slab due to the absence of the folding-back effect. To more intuitively observe the codirectional crossing points, C and C', a magnified image is plotted in Fig. 5(b). The black dashed lines denote the band structure in the absence of magnetoelastic interactions for comparison. Obviously, there exist two veerings between the spin and elastic wave modes for the wave vectors $+k$ and $-k$, owing to the existence of magnetoelastic interactions, which deform the linear dispersions of spin and elastic waves. Moreover, the two veerings are located in different frequency ranges. Similar to the effect of the veering in a hybrid electromechanical medium [76], the propagation of elastic waves in the veering is dampened due to the exchange of energy between the spin and elastic modes [44,45,77]. Thus, within the frequency range of one veering, the elastic waves traveling in one direction are prohibited partially, while the elastic waves propagating in the opposite direction are almost unaffected. These results confirm that the propagation of elastic waves is asymmetric in the homogeneous magnetoelastic slab [78]. It is emphasized that asymmetric propagation arising from the veerings near the codirectional anticrossing points in the homogeneous system are significantly different from the efficient elastic wave isolation resulting from directional band gaps in the vicinity of contradirectional anticrossing points in the periodic system.

APPENDIX D: ASYMMETRIC PROPAGATION OF ELASTIC WAVES NEAR CODIRECTIONAL ANTICROSSING POINTS IN 1D LINEAR MAGNETOELASTIC PC SLABS BY AN EXTERNAL MAGNETOSTATIC FIELD

Figure 6 displays an enlarged image of the codirectional anticrossing points [$C0$ and $C0'$ in Fig. 2(a)] in the 1D linear magnetoelastic PC slabs. It can be seen that two veerings exist between the spin and elastic wave branches for $+k$ and $-k$ due to magnetoelastic interactions when both the wavelengths and frequencies of the spin and elastic waves are close [44,45]. Moreover, the two veerings are

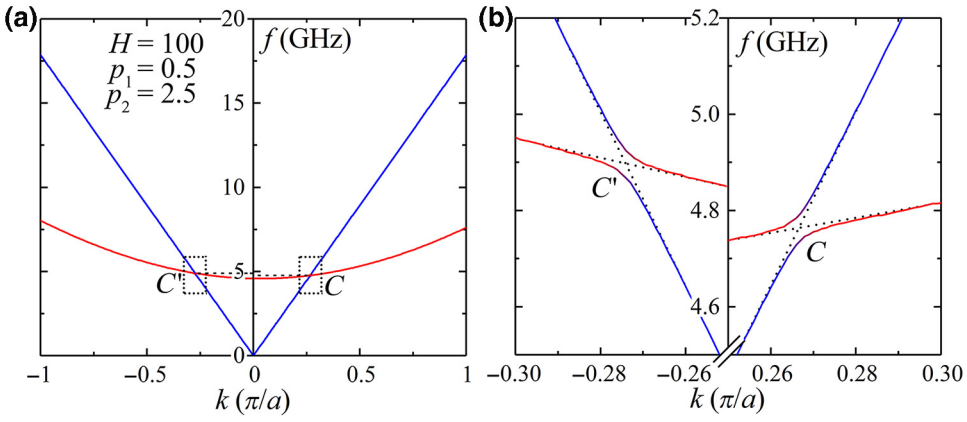

FIG. 5. (a) Band structure of the homogeneous magnetoelastic slab with $H = 100$ kA/m and different surface-spin-pinning parameters, $p_1 = 0.5$ and $p_2 = 2.5$. (b) Magnification of the codirectional anticrossing points, C and C'. Black dashed lines denote the band structure in the absence of magnetoelastic interactions for comparison.

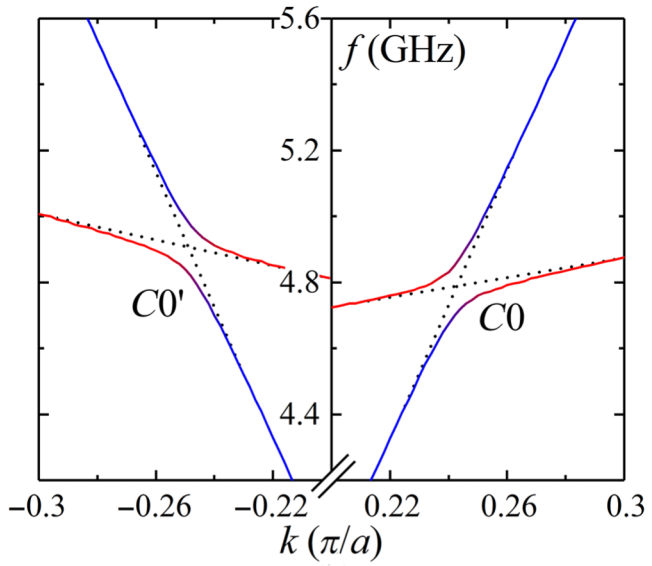

FIG. 6. Magnifications of codirectional anticrossing points [$C0$ and $C0'$ in Fig. 2(a)] in the 1D linear magnetoelastic PC slabs.

located in different frequency ranges because the spin wave dispersion is asymmetric under the simultaneous breaking of the time-reversal and spatial-reversal symmetries of the spin wave subsystem [56–58]. These results demonstrate that the propagation of elastic waves is asymmetric in the frequency range near the codirectional anticrossing points in the 1D linear magnetoelastic PC slabs [78], which is drastically different from the efficient elastic wave isolation near the contradirectional anticrossing points.

APPENDIX E: SYMMETRY ARGUMENT OF NONRECIPROCAL ELASTIC WAVES

A simple symmetry argument [47,79] illustrates the relationship between nonreciprocal elastic waves and breaking of the time-reversal and spatial-inversion symmetries in the 1D magnetoelastic PC slabs. First, for the system with only broken spatial-inversion symmetry, reflecting it in the x_2-x_3 plane changes the wave vector $+k$ to $-k$, but leaves the system invariant, which means that there is $f(+k) = f(-k)$. Second, for the system with broken time-reversal symmetry, reflecting it through the x_2-x_3 plane changes $+k$ to $-k$ and reverses the direction of the external magnetic field because it is an axial vector. If we continue to reflect in the x_1-x_3 plane, the wave vector $-k$ remains unchanged, while the external magnetic field is returned to its original direction, and the positions of the lower and upper surfaces are exchanged. If the lower and upper surface-spin-pinning parameters are the same ($p_1 = p_2$), the system is unchanged by the symmetry operation of the two successive reflections, resulting in $f(+k) = f(-k)$. If $p_1 \neq p_2$, the system is not returned to its original state, which makes it possible for $f(+k) \neq f(-k)$. Therefore, the simultaneous breaking of time-reversal and spatial-inversion symmetries is the necessary factor for the nonreciprocity of elastic waves in a periodic system.

[1] C. W. Chang, D. Okawa, A. Majumdar, and A. Zettl, Solid-State thermal rectifier, Science **314**, 1121 (2006).
[2] B. Liang, X. S. Guo, J. Tu, D. Zhang, and J. C. Cheng, An acoustic rectifier, Nat. Mater. **9**, 989 (2010).
[3] N. Boechler, G. Theocharis, and C. Daraio, Bifurcation-based acoustic switching and rectification, Nat. Mater. **10**, 665 (2011).
[4] C. Coulais, D. Sounas, and A. Alu, Static non-reciprocity in mechanical metamaterials, Nature **542**, 461 (2017).
[5] Y. X. Shen, Y. G. Peng, D. G. Zhao, X. C. Chen, J. Zhu, and X. F. Zhu, One-Way Localized Adiabatic Passage in an Acoustic System, Phys. Rev. Lett. **122**, 094501 (2019).
[6] R. Fleury, D. L. Sounas, C. F. Sieck, M. R. Haberman, and A. Alù, Sound isolation and giant linear nonreciprocity in a compact acoustic circulator, Science **343**, 516 (2014).
[7] Z. Wang, Y. Chong, J. D. Joannopoulos, and M. Soljacic, Observation of unidirectional backscattering-immune topological electromagnetic states, Nature **461**, 772 (2009).
[8] Z. Yang, F. Gao, X. Shi, X. Lin, Z. Gao, Y. Chong, and B. Zhang, Topological Acoustics, Phys. Rev. Lett. **114**, 114301 (2015).
[9] J. W. Dong, X. D. Chen, H. Zhu, Y. Wang, and X. Zhang, Valley photonic crystals for control of spin and topology, Nat. Mater. **16**, 298 (2017).
[10] J. M. Zhao, S. Y. Huo, H. B. Huang, and J. J. Chen, Topological interface states of shear horizontal guided wave in One-dimensional phononic quasicrystal slabs, Phys. Status Solidi RRL **12**, 1800322 (2018).
[11] Y. Ding, Y. Peng, Y. Zhu, X. Fan, J. Yang, B. Liang, X. Zhu, X. Wan, and J. Cheng, Experimental Demonstration of Acoustic Chern Insulators, Phys. Rev. Lett. **122**, 014302 (2019).
[12] S. Y. Huo, J. J. Chen, L. Y. Feng, and H. B. Huang, Pseudospins and topological edge states for fundamental antisymmetric lamb modes in snowflakelike phononic crystal slabs, J. Acous. Soc. Am. **146**, 729 (2019).
[13] M. Terraneo, M. Peyrard, and G. Casati, Controlling the Energy Flow in Nonlinear Lattices: A Model for a Thermal Rectifier, Phys. Rev. Lett. **88**, 094302 (2002).
[14] B. Li, L. Wang, and G. Casati, Thermal Diode: Rectification of Heat Flux, Phys. Rev. Lett. **93**, 184301 (2004).
[15] L. Fan, J. Wang, L. T. Varghese, H. Shen, B. Niu, Y. Xuan, A. M. Weiner, and M. Qi, An all-silicon passive optical diode, Science **335**, 447 (2012).
[16] Y. Shi, Z. Yu, and S. Fan, Limitations of nonlinear optical isolators due to dynamic reciprocity, Nat. Photonics **9**, 388 (2015).
[17] E. Li, B. J. Eggleton, K. Fang, and S. Fan, Photonic aharonov-bohm effect in photon-phonon interactions, Nat. Commun. **5**, 3225 (2014).

[18] J. Kim, M. C. Kuzyk, K. Han, H. Wang, and G. Bahl, Non-reciprocal brillouin scattering induced transparency, Nat. Phys. **11**, 275 (2015).

[19] B. Liang, B. Yuan, and J. C. Cheng, Acoustic Diode: Rectification of Acoustic Energy Flux in one-Dimensional Systems, Phys. Rev. Lett. **103**, 104301 (2009).

[20] S. Lepri and G. Casati, Asymmetric Wave Propagation in Nonlinear Systems, Phys. Rev. Lett. **106**, 164101 (2011).

[21] B. I. Popa and S. A. Cummer, Non-reciprocal and highly nonlinear active acoustic metamaterials, Nat. Commun. **5**, 3398 (2014).

[22] C. Liu, Z. Du, Z. Sun, H. Gao, and X. Guo, Frequency-Preserved Acoustic Diode Model with High Forward-Power-Transmission Rate, Phys. Rev. Appl. **3**, 064014 (2015).

[23] M. B. Zanjani, A. R. Davoyan, A. M. Mahmoud, N. Engheta, and J. R. Lukes, One-way phonon isolation in acoustic waveguides, Appl. Phys. Lett. **104**, 081905 (2014).

[24] G. Trainiti and M. Ruzzene, Non-reciprocal elastic wave propagation in spatiotemporal periodic structures, New J. Phys. **18**, 083047 (2016).

[25] H. Nassar, H. Chen, A. N. Norris, M. R. Haberman, and G. L. Huang, Non-reciprocal wave propagation in modulated elastic metamaterials, Proc. R. Soc. A **473**, 20170188 (2017).

[26] Y. Wang, B. Yousefzadeh, H. Chen, H. Nassar, G. Huang, and C. Daraio, Observation of Nonreciprocal Wave Propagation in a Dynamic Phononic Lattice, Phys. Rev. Lett. **121**, 194301 (2018).

[27] Y. Chen, X. Li, H. Nassar, A. N. Norris, C. Daraio, and G. Huang, Nonreciprocal Wave Propagation in a Continuum-Based Metamaterial with Space-Time Modulated Resonators, Phys. Rev. Appl. **11**, 064052 (2019).

[28] F. Ruesink, M. A. Miri, A. Alu, and E. Verhagen, Nonreciprocity and magnetic-free isolation based on optomechanical interactions, Nat. Commun. **7**, 13662 (2016).

[29] Z. Shen, Y. L. Zhang, Y. Chen, C. L. Zou, Y. F. Xiao, X. B. Zou, F. W. Sun, G. C. Guo, and C. H. Dong, Experimental realization of optomechanically induced non-reciprocity, Nat. Photonics **10**, 657 (2016).

[30] H. Xu, L. Jiang, A. A. Clerk, and J. G. E. Harris, Non-reciprocal control and cooling of phonon modes in an optomechanical system, Nature **568**, 65 (2019).

[31] E. A. Kittlaus, N. T. Otterstrom, P. Kharel, S. Gertler, and P. T. Rakich, Non-reciprocal interband brillouin modulation, Nat. Photonics **12**, 613 (2018).

[32] A. V. Poshakinskiy and A. N. Poddubny, Phonoritonic Crystals with a Synthetic Magnetic Field for an Acoustic Diode, Phys. Rev. Lett. **118**, 156801 (2017).

[33] M. Faraday, On the magnetization of light and the illumination of magnetic lines of force, Phil. Trans. R. Soc. **134**, 104 (1846).

[34] M. Atatüre, J. Dreiser, A. Badolato, and A. Imamoglu, Observation of Faraday rotation from a single confined spin, Nat. Phys. **3**, 101 (2007).

[35] F. D. M. Haldane and S. Raghu, Possible Realization of Directional Optical Waveguides in Photonic Crystals with Broken Time-Reversal Symmetry, Phys. Rev. Lett. **100**, 013904 (2008).

[36] I. Crassee, J. Levallois, A. L. Walter, M. Ostler, A. Bostwick, E. Rotenberg, T. Seyller, D. van der Marel, and A. B. Kuzmenko, Giant Faraday rotation in single- and multilayer graphene, Nat. Phys. **7**, 48 (2010).

[37] W. K. Tse and A. H. MacDonald, Giant Magneto-Optical Kerr Effect and Universal Faraday Effect in Thin-Film Topological Insulators, Phys. Rev. Lett. **105**, 057401 (2010).

[38] L. Bi, J. Hu, P. Jiang, D. H. Kim, G. F. Dionne, L. C. Kimerling, and C. A. Ross, On-chip optical isolation in monolithically integrated non-reciprocal optical resonators, Nat. Photonics **5**, 758 (2011).

[39] D. Dominguez, L. Bulaevskii, B. Ivlev, M. Maley, and A. R. Bishop, Interaction of Vortex Lattice with Ultrasound and the Acoustic Faraday Effect, Phys. Rev. Lett. **74**, 2579 (1995).

[40] Y. Lee, T. M. Haard, W. P. Halperin, and J. A. Sauls, Discovery of the acoustic Faraday effect in superfluid ^{3}He-B, Nature **400**, 431 (1999).

[41] A. Sytcheva, U. Löw, S. Yasin, J. Wosnitza, S. Zherlitsyn, P. Thalmeier, T. Goto, P. Wyder, and B. Lüthi, Acoustic Faraday effect in $Tb_3Ga_5O_{12}$, Phys. Rev. B **81**, 214415 (2010).

[42] G. T. Rado and J. R. Webrtman, Spin-wave resonance in a ferromagnetic metal, J. Phys. Chem. Solids **11**, 315 (1959).

[43] R. E. Camley and R. Q. Scott, Surface magnetoelastic waves in the presence of exchange interactions and pinning of surface spins, Phys. Rev. B **17**, 4327 (1978).

[44] P. Graczyk and M. Krawczyk, Coupled-mode theory for the interaction between acoustic waves and spin waves in magnonic-phononic crystals: Propagating magnetoelastic waves, Phys. Rev. B **96**, 024407 (2017).

[45] C. Kittel, Interaction of spin waves and ultrasonic waves in ferromagnetic crystals, Phys. Rev. **110**, 836 (1958).

[46] R. E. Camley and A. A. Maradudin, Power flow in magnetoelastic media, Phys. Rev. B **24**, 1255 (1981).

[47] R. E. Camley, Nonreciprocal surface waves, Surf. Sci. Rep. **7**, 103 (1987).

[48] M. S. Kushwaha, P. Halevi, L. Dobrzynski, and B. Djafari-Rouhani, Acoustic Band Structure of Periodic Elastic Composites, Phys. Rev. Lett. **71**, 2022 (1993).

[49] J. J. Chen, B. Bonello, and Z. L. Hou, Plate-mode waves in phononic crystal thin slabs: Mode conversion, Phys. Rev. E **78**, 036609 (2008).

[50] T. T. Wu, Z. G. Huang, and S. Lin, Surface and bulk acoustic waves in two-dimensional phononic crystal consisting of materials with general anisotropy, Phys. Rev. B **69**, 094301 (2004).

[51] R. E. Camley, Magnetoelastic waves in a ferromagnetic film on a nonmagnetic substrate, J. Appl. Phys. **50**, 5272 (1979).

[52] P. Graczyk, J. Kłos, and M. Krawczyk, Broadband magnetoelastic coupling in magnonic-phononic crystals for high-frequency nanoscale spin-wave generation, Phys. Rev. B **95**, 104425 (2017).

[53] N. Zhen, Y. S. Wang, and C. Zhang, Surface/interface effect on band structures of nanosized phononic crystals, Mech. Res. Commun. **46**, 81 (2012).

[54] N. Zhen, Y. S. Wang, and C. Zhang, Bandgap calculation of in-plane waves in nanoscale phononic crystals taking account of surface/interface effects, Phys. E **54**, 125 (2013).
[55] B. R. Mace and E. Manconi, Wave motion and dispersion phenomena: Veering, locking and strong coupling effects, J. Acoust. Soc. Am. **131**, 1015 (2012).
[56] A. Gukasov, Left right asymmetry in polarised neutron scattering, Phys. B **267**, 97 (1999).
[57] M. Mruczkiewicz, M. Krawczyk, G. Gubbiotti, S. Tacchi, Y. A. Filimonov, D. V. Kalyabin, I. V. Lisenkov, and S. A. Nikitov, Nonreciprocity of spin waves in metallized magnonic crystal, New J. Phys. **15**, 113023 (2013).
[58] G. Gitgeatpong, Y. Zhao, P. Piyawongwatthana, Y. Qiu, L. W. Harriger, N. P. Butch, T. J. Sato, and K. Matan, Nonreciprocal Magnons and Symmetry-Breaking in the Noncentrosymmetric Antiferromagnet, Phys. Rev. Lett. **119**, 047201 (2017).
[59] T. Nomura, X. X. Zhang, S. Zherlitsyn, J. Wosnitza, Y. Tokura, N. Nagaosa, and S. Seki, Phonon Magnetochiral Effect, Phys. Rev. Lett. **122**, 145901 (2019).
[60] M. F. Lewis and E. Patterson, Acoustic-Surface-Wave isolator, Appl. Phys. Lett. **20**, 276 (1972).
[61] J. Cha and C. Daraio, Electrical tuning of elastic wave propagation in nanomechanical lattices at MHz frequencies, Nat. Nanotechnol. **13**, 1016 (2018).
[62] M. Yan, J. Lu, F. Li, W. Deng, X. Huang, J. Ma, and Z. Liu, On-chip valley topological materials for elastic wave manipulation, Nat. Mater. **17**, 993 (2018).
[63] J. Cha, K. W. Kim, and C. Daraio, Experimental realization of on-chip topological nanoelectromechanical metamaterials, Nature **564**, 229 (2018).
[64] H. Puszkarski, Quantum theory of spin wave resonance in thin ferromagnetic films. I. spin waves in thin films, part 2: Spin-wave resonance spectrum, Acta Phys. Polon. A **38**, 217 and 899 (1970).
[65] H. Puszkarski, Theory of surface states in spin wave resonance, Progr. Surf. Sci. **9**, 191 (1979).
[66] H. Puszkarski and M. Kasperski, On the interpretation of the angular dependence of the main FMR/SWR line in ferromagnetic thin films, Acta Phys. Polon. **121**, 1165 (2012).
[67] J. T. Yu, R. A. Turk, and P. E. Wigen, Exchange-dominated surface spin waves in thin yttrium-iron-garent films, Phys. Rev. B **11**, 420 (1975).
[68] P. E. Wigen and H. Puszkarski, Microscopic model for the tensorial surface anisotropy field observed in thin yitrium-iron garnet film spin-wave resonance, Solid State Commun. **18**, 363 (1976).
[69] H. Puszkarski, Complex angle dependence of the surface pinning parameter in magnetic thin films, Solid State Commun. **22**, 563 (1977).
[70] A. P. Cracknell and H. Puszkarski, Symmetry properties of the surface pinning parameter in magnetic thin films, Solid State Commun. **28**, 891 (1978).
[71] A. R. Ferchmin and H. Puszkarski, Existence conditions of surface spin waves in ferromagnetic nanowires and nanoparticles, J. Appl. Phys. **90**, 5335 (2001).
[72] H. Puszkarski and P. Tomczak, Spin-wave resonance model of surface pinning in ferromagnetic semiconductor (Ga, Mn)As thin films, Sci. Rep. **4**, 6135 (2014).
[73] S. H. Mousavi, A. B. Khanikaev, and Z. Wang, Topologically protected elastic waves in phononic metamaterials, Nat. Commun. **6**, 8682 (2015).
[74] T. Ma, A. B. Khanikaev, S. H. Mousavi, and G. Shvets, Guiding Electromagnetic Waves Around Sharp Corners: Topologically Protected Photonic Transport in Metawaveguides, Phys. Rev. Lett. **114**, 127401 (2015).
[75] M. Miniaci, R. K. Pal, R. Manna, and M. Ruzzene, Valley-based splitting of topologically protected helical waves in elastic plates, Phys. Rev. B **100**, 024304 (2019).
[76] A. E. Bergamini, M. Zündel, E. A. Flores Parra, T. Delpero, M. Ruzzene, and P. Ermanni, Hybrid dispersive media with controllable wave propagation: A new take on smart materials, J. Appl. Phys. **118**, 154310 (2015).
[77] A. Kamra, H. Keshtgar, P. Yan, and G. E. W. Bauer, Coherent elastic excitation of spin waves, Phys. Rev. B **91**, 104409 (2015).
[78] A. A. Maznev, A. G. Every, and O. B. Wright, Reciprocity in reflection and transmission: What is a "phonon diode"?, Wave Motion **50**, 776 (2013).
[79] R. Q. Scott and D. L. Mills, Propagation of surface magnetoelastic waves on ferromagnetic crystal substrates, Phys. Rev. B **15**, 3545 (1977).